Adaptive Tracking Control for Diffractive Film Based on Nonlinear Sliding Mode

MA Songjing[1], *SONG Xiangshuai*[1*], *LI Jun*[2], *SUN Yuqi*[1], *WANG Yuyao*[1]

1. College of Aerospace and Civil Engineering, Harbin Engineering University, Harbin 150001, P.R. China;

2. Marine Design and Research Institute of China, Shanghai 210110, P.R. China

Abstract: A nonlinear sliding mode adaptive controller for a thin-film diffractive imaging system is designed to achieve accurate pointing direction over the attitude of subarrays in large-diameter mirror arrays. The kinematics and dynamics equations based on error quaternion and angular velocity are derived, and a diffractive thin-film sub-mirror array controller is designed to point precisely. Moreover, the global stability of the controller is proved by the Lyapunov method. Since the controller can adaptively identify the inertia matrix of each sub-mirror system, it is robust to bounded disturbances and changes in inertia parameters. At the same time, the continuous arctangent function is introduced, which is effectively anti-chattering. The simulation results show that the designed controller can ensure the accurate tracking of the diffractive film in each sub-mirror in the presence of rotational inertia matrix uncertainty and various disturbances.

Key words: attitude tracking; sliding mode control; diffraction imaging; optical imaging system; Lyapunov function

CLC number: V414.5　　**Document code:** A　　**Article ID:** 1005-1120(2022)06-0696-11

0 Introduction

The increasing focus length and payload lens diameter caused by the demands of ever-increasing Earth observation resolution have exceeded the launching ability of rockets[1]. As a new type of imaging technology, the diffractive thin-film imaging technology has the advantages of lighter weight, variable surface shape, easier to be folded and unfolded, lower surface density, and lower cost compared with traditional optical imaging payloads[2-3]. The diffractive thin film is one of the most promising practical approaches for imaging systems to solve the problem of ultra-large aperture and ultra-light load imaging systems in space.

In 1998, the Eyeglass project, whose telescope system consists of an objective lens satellite and an eyepiece satellite, was proposed by the Lawrence Livermore National Laboratory (LLNL) in the United States. And the feasibility of diffraction imaging technology was proved by the ground prototype[4-5]. In 2010, the membrane optical imager real-time exploitation (MORIE) satellite research program, which is greatly improved based on the "Eyeglass Program", was announced by the Defense Advanced Research Projects Agency (DARPA)[6-7].

The diffraction imaging system consists of an imaging satellite and a diffraction film satellite. The diffractive film satellite is equipped with a film primary mirror which is covered with small nanoscale etched holes for imaging based on the diffraction principle. The rest of the imaging system is built on the imaging satellite. On the one hand, due to different orbital altitudes of binary satellites, the diffractive film sub-mirrors need to adjust its pointing in real-time to ensure the quality of images. On the other hand, the diffraction imaging system is in a complex space environment, where disturbing factors such as solar light pressure, non-spherical perturbation of the Earth, and atmospheric drag also have impact

on the pointing accuracy. Therefore, high accuracy tracking and pointing control of diffraction films is essential.

The control of the separate diffractive imaging system is the key to ensuring the relative attitude pointing, so it has gained extensive interest in recent years. The representative one is a set of orbital parameters of the co-located diffraction imaging system designed by Sun et al.[8], which also showed the feasibility of post-disaster remote sensing. The designed co-located diffractive satellite system can simultaneously provide an essential reference for post-disaster emergency response. Presently, the relative control of diffraction imaging satellites mainly draws on the relative attitude control of the binary satellite formation. Considering the uncertainty of angular velocity, the impulse variance control method for the binary satellite based on the observer-based was proposed, which solved the stability problems with parameter uncertainty, pole constraint, variance constraint, and limited thrust[9-10]. An adaptive sliding mode control scheme is designed to solve the high-precision tracking control of the formation spacecraft[11-12]. Combined with the characteristics of the integral sliding mode segment, an adaptive integral sliding mode control law was proposed, which solved the problem of excessive adaptation of switching gain in the attitude tracking control of spacecraft[13]. Sun et al.[14] designed a robust adaptive feedback-limited controller, where the modified Rodrigues parameters were used to describe the attitude tracking dynamics model. Xu et al.[15] used the square root volumetric Kalman filter to estimate the relative position and calculate the desired attitude. Correspondingly the error attitude dynamics equation was described based on the modified Rodrigues parameter, and the backstepping adaptive control law was used to control the pointing and tracking of the spacecraft. Yin[16] proposed a multi-loop recursive tracking attitude control strategy, and the integral term of attitude tracking error was introduced into the attitude tracking dynamic system so that the structure of the attitude tracking system was changed.

For diffraction imaging control of the diffractive film, there are few archives introducing conception and design. Hence, we take the satellite attitude control method as a reference to implement film-pointing control. In order to improve the convergence rate and system life, a variable structure sliding mode control method for satellite attitude maneuver was proposed, where the constraint relationship between the control parameters and the system performance was given to prevent the system state from exceeding its upper bound[17]. A method of finite time adaptive integral sliding mode controller was proposed to guarantee the spacecraft attitude tracking target attitude[18]. In the presence of uncertain parameters and unknown inputs, a robust control method was proposed for rigid spacecraft attitude stabilization using the state-dependent indirect Chebyshev pseudospectral method[19], and the design of a passivity-based adaptive robust control for attitude tracking of a three-axis satellite was investigated[20]. Although these methods can well solve the relative attitude control problem of the double-satellite formation, the controller of thin-film mirror array satellites with limited motion of thin-film mirrors for diffraction imaging has not been studied.

In this paper, we will analyze the desired pointing angle for high-precision attitude tracking control of the diffractive film sub-mirror, build an attitude tracking error model, and following this, the diffractive thin-film sub-mirror array control schemes will be designed. This paper is organized as follows. Section 1 states the model establishment of the diffraction imaging system. The primary research is developed in Section 2, in which the adaptive controller of a diffractive thin-film sub-mirror array is proposed to achieve highly accurate tracking in finite time. And the stability of the proposed controller is proven using the Lyapunov stable theory. Then, the numerical results are simulated and the PD controller is introduced for comparison tests with the controller proposed in Section 3. Finally, conclusions are given in Section 4.

1   Diffraction Imaging System Model

1. 1   Diffraction imaging system description

The diffraction imaging system consists of the thin-film diffraction mirror array satellite and imaging satellite, which maintains a formation configuration to realize the high-precision imaging function of a heterogeneous binary satellite. The imaging satellite is treated as a particle to simplify the model. Each diffractive thin-film sub-mirror rotates around its pitch axis so that the plane of each thin-film sub-mirror is perpendicular to the optical imaging path, thereby realizing real-time tracking and orientation of the imaging satellite. The imaging position relationship is shown in Fig.1.
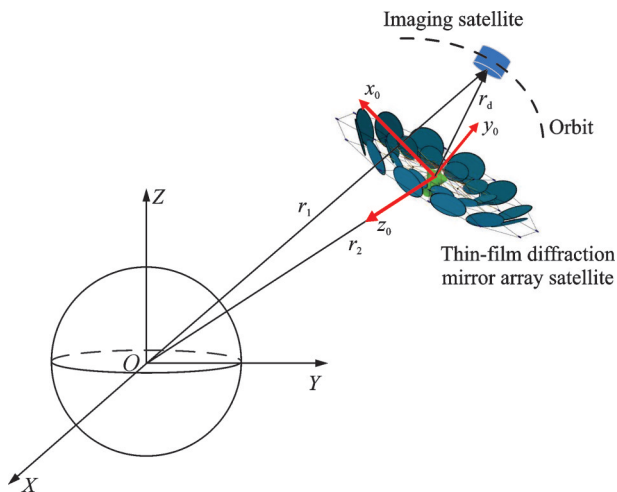

Fig.1   Binary satellite thin film diffraction imaging system

1. 2   Diffraction mirror array satellite model

In this paper, the research object is the thin-film diffractive mirror array satellite for diffraction imaging of nano-scale etched pinholes. It is mainly composed of three parts: Central body structure, diffractive film sub-mirror array, and truss. The diffractive film sub-mirror, which is unfolded and flattened by the truss, can be twisted and adjusted independently[21-22]. The sub-mirrors orient to the imaging satellite by rotating around their pitch axis. As shown in Fig.1, the earth-centered inertial (ECI) frame $O\text{-}XYZ$ is a coordinate system, in which the origin is the center of mass of the Earth, the XY plane is the Earth's equatorial plane at the moment of J2000, and the X-axis points to the equinox at the

moment of J2000. The spatial configuration of the thin-film diffraction mirror array satellite and diffractive film sub-mirror system are shown in Fig.2. The thin-film diffractive mirror array satellite consists of 24 diffractive thin-film sub-mirrors in the inner and outer circles. To facilitate controller design, the outermost mirror pointed by the X-axis of the thin-film diffractive mirror array satellite body coordinate system is numbered as α_1, and other mirrors are numbered counterclockwise, as shown in Fig.2. $r_{mi}^{\circ}(i = 1, 2, \cdots, n)$ is the distance vector of the sub-mirror from its centroid in the thin-film diffraction satellite body coordinate system, where the subscript mi is ith diffractive thin-film sub-mirror and n is the total number of mirrors in the thin-film diffraction mirror array satellite.
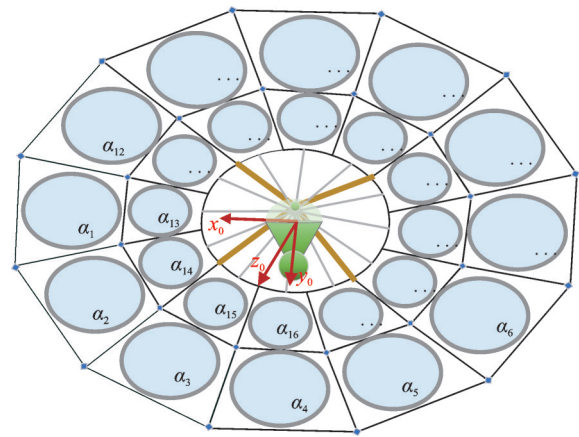

Fig.2   Thin-film diffraction mirror array satellite sub-array system

1. 3   Desired attitude angle model of diffractive film

The desired attitude of the diffractive film should be perpendicular to the optical path of the imaging satellite. In the process of high-precision imaging, the model is simplified for specific problems under certain assumptions to derive the desired attitude angle. The basic assumptions are given as follows.

(1) In the process of maintaining the formation configuration, the imaging satellites and the thin-film diffraction mirror array satellites are oriented to the ground, whose body coordinate system coincides with the orbital system.

(2) The imaging satellite can be regarded as a

particle whose center of mass coincides with the geo-metric center.

(3) The centroid displacement of the thin-film diffractive mirror array satellite caused by the rotation of the diffractive thin-film sub-mirror is a negligibly small amount.

The desired attitude information of each diffractive thin-film sub-mirror system is related to the relative distance vector of the thin-film diffractive mirror array satellite and the imaging satellite.

The relative distance vector of the binary satellite in the ECI frame $O\text{-}XYZ$ can be expressed as

$$r_d = r_1 - r_2 \qquad (1)$$

where r_1 and r_2 represent the vectors from the imaging satellite and the thin film diffraction mirror array satellite to the center of the earth in the ECI frame $O\text{-}XYZ$, respectively.
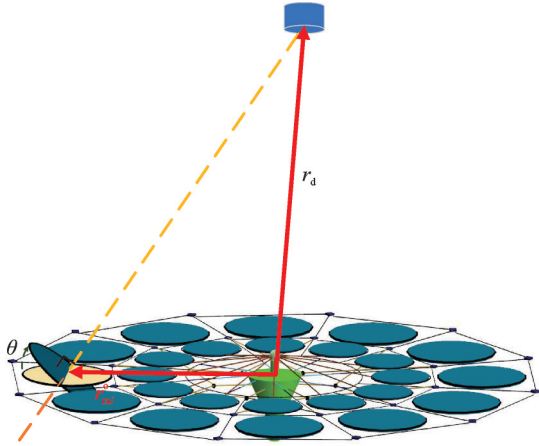

Fig.3 Desired pointing angle of diffractive film sub-mirror system

The distance vector r_{si} from the imaging satellite to the centroid of the diffractive film sub-mirror can be expressed as

$$r_{si} = r_d - L_{eo} \cdot r_{mi}^o \quad i = 1, 2, \cdots, n \qquad (2)$$

where L_{eo} is the coordinate transformation from the orbit reference frame to the ECI frame[23]. It can be written as

$$L_{eo} = L_z(-\Omega) L_x\left(\frac{\pi}{2} - i\right) L_y\left(\frac{\pi}{2} + u\right) =$$
$$\begin{bmatrix} -c\Omega su - s\Omega cicu & -s\Omega si & s\Omega cisu - c\Omega cu \\ c\Omega cicu - s\Omega su & c\Omega si & -s\Omega cu - c\Omega cisu \\ cusi & -ci & -sisu \end{bmatrix} \quad (3)$$

where c and s denote $\cos(\cdot)$ and $\sin(\cdot)$, respectively; Ω is the right ascension of the ascending node of the orbit, i the inclination of the orbit, $u = f + \omega$ a latitude parameter representing the position of the spacecraft relative to the ascending node, f the true anomaly, and ω the argument of perigee. The expected pointing angle of each diffractive thin-film sub-mirror α_i in the high-precision imaging configuration maintaining mode is shown in Fig.3, which can be expressed as

$$\theta_i = \arccos\left(\frac{r_{si} \cdot r_{mi}}{|r_{si}| \cdot |r_{mi}|}\right) \qquad (4)$$

1.4 Attitude tracking error model of diffractive film

The relative attitude error kinematics and dynamics models of diffractive thin-film sub-mirrors represented by quaternions can be established as[24]

$$J_i \dot{\omega}_{ei} = -(\omega_{ei} + C_i \omega_{ti})^\times J_i (\omega_{ei} + C_i \omega_{ti}) + J_i(\omega_{ei}^\times C_i \omega_{ti} + C_i \dot{\omega}_{ti}) + T_i + Td_i \qquad (5)$$

$$\begin{cases} \dot{q}_{ei0} = -\dfrac{1}{2} q_{ei}^T \omega_{ei} \\ \dot{q}_{ei} = \dfrac{1}{2}(q_{ei0} I_3 + q_{ei}^\times) \omega_{ei} \end{cases} \qquad (6)$$

where $i = 1, 2, \cdots, n$ represents the ith diffractive thin-film sub-mirror, $J_i \in \mathbf{R}^{3\times3}$ the moment of inertia matrix, and ω_{ti} desired attitude angular velocity; $\omega_{ei} = \omega_{bi} - C_i \omega_{ti}$ denotes the angular velocity error between the actual attitude and the desired attitude, where ω_{bi} represents the attitude angular velocity, and the specific expression of the attitude transformation matrix C_i is $C_i = (q_{ei0}^2 - q_{ei}^T q_{ei}) I_3 + 2 q_{ei} q_{ei}^T - 2 q_{ei0} q_{ei}^\times$ with $\|C_i\| = 1$, $C_i^T C_i = 1$, $\dot{C}_i = -\omega_{ei}^\times C_i$, $(\cdot)^\times$ denotes a 3×3 skew-symmetric matrix, $q_{ei} = [q_{ei1}, q_{ei2}, q_{ei3}]^T$ is the vector part of the quaternion for the attitude error. T_i and Td_i are the control moment and bounded disturbance, respectively. I_3 is the identity matrix. The attitude tracking error $Q_{ei} = [q_{ei0}, q_{ei}^T]^T$ denotes the relative attitude error from the actual attitude to the desired attitude, which can be obtained as

$$Q_{ei} = Q_{ti}^{-1} \otimes Q_{bi} = \begin{bmatrix} q_{ti0} & q_{ti1} & q_{ti2} & q_{ti3} \\ -q_{ti1} & q_{ti0} & q_{ti3} & -q_{ti2} \\ -q_{ti2} & -q_{ti3} & q_{ti0} & q_{ti1} \\ -q_{ti3} & q_{ti2} & -q_{ti1} & q_{ti0} \end{bmatrix} \begin{bmatrix} q_{bi0} \\ q_{bi1} \\ q_{bi2} \\ q_{bi3} \end{bmatrix} \qquad (7)$$

where Q_{bi} and Q_{ti} represent the actual and desired at-

titude quaternion, respectively. $\otimes$ represents the quaternion multiplication.

2 Thin-Film Diffraction Sub-Array Mirror Controller Design

In this section, we propose a novel nonlinear synovial surface with the inverse tangent signum function. Then, we design the adaptive attitude tracking control schemes for the thin-film diffraction sub-array mirror system in the presence of inertia uncertainties and external disturbances[25]. The algorithm is based on a nonlinear sliding mode and has the advantages of finite time tracking, fast, accurate, anti-chattering, suppressing inertial uncertainty, and adaptively identifying the upper bound of interference. The traditional symbolic sliding mode variable structure control system suffers from severe jitter and vibration. The introduction of an arctangent function eliminates the jitter caused by the sign function and ensures fast global convergence of the system state on the sliding mode plane.

For each sub-mirror in the thin-film diffractive mirror array satellite, the nonlinear synovial surface can be defined as

$$s_i = \boldsymbol{\omega}_{ei} + \boldsymbol{K}\left(\frac{2}{\pi}\arctan q_{ei}\right) \qquad (8)$$

where $\boldsymbol{K}$ is the positive definite diagonal matrix, and $\arctan q_{ei} = [\arctan q_{ei1} \ \arctan q_{ei2} \ \arctan q_{ei3}]^T$. The attitude error quaternion has the property of $q_{ei0}^2 + \boldsymbol{q}_{ei}^T \cdot \boldsymbol{q}_{ei} = 1$, we have $\forall t \geqslant 0, |q_{ei_j}| \leqslant 1, j = 1, 2, 3.$

$$q_{ei_j} \arctan q_{ei_j} > 0, q_{ei_j} \neq 0 \qquad \arctan 0 = 0 \qquad (9)$$

For $\forall \xi \in \mathbf{R}$ and $\forall a \in \mathbf{R}$, the arctangent function $\arctan \xi$ yields

$$\xi \arctan \xi = |\xi| \arctan |\xi| \qquad (10)$$

$$\xi \arctan(|a|\xi) > 0, \xi \neq 0 \qquad \arctan 0 = 0 \quad (11)$$

$$\frac{\mathrm{d}}{\mathrm{d}t}\arctan \xi = \frac{1}{1+\xi^2}\dot{\xi} \qquad (12)$$

Assuming that the moment of inertia $\boldsymbol{J}_i$ of the diffractive film sub-mirror α_i is an unknown positive definite symmetric constant matrix[26]. The disturbance torque $\boldsymbol{Td}_i$ is bounded. The estimated error of the inertia parameter can be defined as

$$\bar{\boldsymbol{j}}_i = \boldsymbol{j}_i - \tilde{\boldsymbol{j}}_i \qquad (13)$$

where $\boldsymbol{j}_i = [J_{i11} \ J_{i22} \ J_{i33} \ J_{i12} \ J_{i13} \ J_{i23}]^T$ represents the inertia parameter of the diffractive film submirror numbered α_i, whose estimated inertia parameter is $\tilde{\boldsymbol{j}}_i = [\tilde{J}_{i11} \ \tilde{J}_{i22} \ \tilde{J}_{i33} \ \tilde{J}_{i12} \ \tilde{J}_{i13} \ \tilde{J}_{i23}]^T$.

It is known from the assumption that the inertia parameter of the diffractive film sub-mirror is an unknown constant, then there is $\bar{\boldsymbol{j}}_i = -\tilde{\boldsymbol{j}}_i$.

The linear operator is defined as

$$L(\boldsymbol{\xi}) = \begin{bmatrix} \xi_1 & 0 & 0 & \xi_2 & \xi_3 & 0 \\ 0 & \xi_2 & 0 & \xi_1 & 0 & \xi_3 \\ 0 & 0 & \xi_3 & 0 & \xi_1 & \xi_2 \end{bmatrix} \qquad (14)$$

For $\forall \boldsymbol{\xi} = [\xi_1 \ \xi_2 \ \xi_3]^T \in \mathbf{R}^3$, there is $\boldsymbol{J}\boldsymbol{\xi} = L(\boldsymbol{\xi})\boldsymbol{j}$.

Multiplying the derivative of Eq.(8) to the left by $\boldsymbol{J}_i$ and substituting Eqs.(5) and (6) into it obtains

$$\boldsymbol{J}_i \dot{s}_i = \boldsymbol{T}_i + \boldsymbol{Td}_i - (\boldsymbol{\omega}_{ei} + \boldsymbol{C}_i\boldsymbol{\omega}_{ti})^{\times} \boldsymbol{J}_i(\boldsymbol{\omega}_{ei} + \boldsymbol{C}_i\boldsymbol{\omega}_{ti}) +$$
$$\boldsymbol{J}_i(\boldsymbol{\omega}_{ei}^{\times}\boldsymbol{C}_i\boldsymbol{\omega}_{ti} - \boldsymbol{C}_i\dot{\boldsymbol{\omega}}_{ti}) + \boldsymbol{J}_i\boldsymbol{K}\frac{1}{\pi(1+q_{ei}^2)}(q_{ei0}\boldsymbol{I}_3 + \boldsymbol{q}_{ei}^{\times})\boldsymbol{\omega}_{ei} \qquad (15)$$

where $\dfrac{1}{1+q_{ei}^2} = \mathrm{diag}\left(\dfrac{1}{1+q_{ei1}^2}, \dfrac{1}{1+q_{ei2}^2}, \dfrac{1}{1+q_{ei3}^2}\right)$.

Applying the linear operator $L: \mathbf{R}^3 \to \mathbf{R}^{3\times 6}$,

$$\boldsymbol{F}_i = -(\boldsymbol{\omega}_{ei} + \boldsymbol{C}_i\boldsymbol{\omega}_{ti})^{\times}L(\boldsymbol{\omega}_{ei} + \boldsymbol{C}_i\boldsymbol{\omega}_{ti}) + L(\boldsymbol{\omega}_{ei}^{\times}\boldsymbol{C}_i\boldsymbol{\omega}_{ti} - \boldsymbol{C}_i\dot{\boldsymbol{\omega}}_{ti}) + L\boldsymbol{K}\frac{1}{\pi(1+q_{ei}^2)}(q_{ei0}\boldsymbol{I}_3 + \boldsymbol{q}_{ei}^{\times})\boldsymbol{\omega}_{ei} \qquad (17)$$

Eq.(15) is simplified as

$$\boldsymbol{J}_i \dot{s}_i = \boldsymbol{F}_i \boldsymbol{j}_i + \boldsymbol{T}_i + \boldsymbol{Td}_i \qquad (16)$$

where

Considering the attitude tracking system described with an unknown inertia matrix and disturbance moment, if Eq.(18) is satisfied, the robust adaptive control law expressed in Eq.(19) and the parameter adaptive adjustment law expressed in

Eq.(20) can ensure that $\bar{\boldsymbol{j}}_i$ and $\overline{\boldsymbol{Td}}_{X i}$ are uniformly ultimately bounded (UUB). That is $\lim\limits_{t \to \infty} \boldsymbol{q}_{ei}(t) = 0$ and $\lim\limits_{t \to \infty} \boldsymbol{\omega}_{ei}(t) = 0$, the error angular velocity $\boldsymbol{\omega}_{ei}$ and the error quaternion $\boldsymbol{q}_{ei}$ of each diffractive thin-

film sub-mirror asymptotically converge into zero[27].

$$\widetilde{Td}_{Xi}(0) > 0 \tag{18}$$

$$T_i = -F_i \tilde{j}_i - \frac{2k}{\pi} \widetilde{Td}_{Xi} \arctan\big((\varepsilon t + \sigma)s_i\big) \tag{19}$$

$$\dot{\tilde{j}}_i = \gamma F_i^{T} s_i, \quad \dot{\widetilde{Td}}_{Xi} = \tau \| s_i \|_{1\,Xi} \tag{20}$$

where ε, σ and τ are undetermined constants; $k = \mathrm{diag}(k_1, k_2, k_3)$, $k_l > 0 (l=1, 2, 3)$; $\widetilde{Td}_{Xi}$ is an esti-

mate of Td_{Xi}; $\overline{Td}_{Xi}$ is estimation error, which is defined as $\overline{Td}_{Xi} = Td_{Xi} - \widetilde{Td}_{Xi}$; $\widetilde{Td}_{Xi}(0)$ is the estimated initial value of $\widetilde{Td}_{Xi}$; $\gamma \in \mathbf{R}^{6 \times 6}$ represents the positive definite diagonal matrix.

Proof

The following Lyapunov candidate function is selected as

$$V = \frac{1}{2} s_i^{T} J_i s_i + \frac{1}{2} \bar{j}_i^{T} \gamma^{-1} \bar{j}_i + \frac{1}{2\tau} \overline{Td}_{Xi}^{2} \tag{21}$$

$$\dot{V}_i = s_i^{T} J_i \dot{s}_i - \bar{j}_i^{T} \gamma \dot{\bar{j}}_i - \frac{1}{\tau} \overline{Td}_{Xi} \dot{\widetilde{Td}}_{Xi} = s_i^{T}\big(F_i \tilde{j}_i + T_i + Td_i\big) + \bar{j}_i^{T} \gamma\big(\gamma^{-1} F_i^{T} s_i - \dot{\bar{j}}_i\big) - \frac{1}{\tau} \overline{Td}_{Xi} \dot{\widetilde{Td}}_{Xi} \leqslant$$

$$s_i^{T}\big(F_i \tilde{j}_i + T_i\big) + \| s_i \|_1 \big(\overline{Td}_{Xi} + \widetilde{Td}_{Xi}\big) + \bar{j}_i^{T} \gamma^{-1}\big(\gamma F_i^{T} s_i - \dot{\bar{j}}_i\big) - \frac{1}{\tau} \overline{Td}_{Xi} \dot{\widetilde{Td}}_{Xi} \tag{22}$$

where $\dot{\bar{j}}_i = -\dot{\tilde{j}}_i$ and $\dot{\overline{Td}}_{Xi} = -\dot{\widetilde{Td}}_{Xi}$.

Inserting Eqs.(10, 19) into Eq.(22) yields

$$\dot{V}_i \leqslant -\left(\frac{2}{\pi} \sum_{l=1}^{3} k_{il} | s_{il} | \arctan\big((\varepsilon t + \sigma)| s_{il} |\big) - \right.$$

$$\left. \sum_{i=1}^{3} | s_{il} | \right) \widetilde{Td}_{Xi}, \quad \widetilde{Td}_{Xi} > 0 \tag{23}$$

When $|s_{il}| \geqslant \dfrac{1}{\varepsilon t + \sigma} \arctan \dfrac{\pi}{2k_{il}}$ there

is $\left(\dfrac{2}{\pi} \displaystyle\sum_{l=1}^{3} k_{il} | s_{il} | \arctan(\varepsilon t + \sigma)| s_{il} | - \displaystyle\sum_{l=1}^{3} | s_{il} | \right) \geqslant 0.$

In addition, when $|s_{il}| \geqslant \dfrac{1}{\varepsilon t + \sigma} \arctan \dfrac{\pi}{2k_{il}}$

there is $\dot{V}_i \leqslant 0$. To sum up, when $t \to \infty$, $s_i \to 0$, $\omega_{ei} \to 0$, $q_{ei} \to 0$, for each diffractive thin-film sub-mirror, $\dot{V}_i$ is semi-negative definite, V_i is radially unbounded, and s_i, $\bar{j}_i$, $\overline{Td}_{Xi}$ are UUB.

3   Numerical Simulations

The diffractive thin-film sub-mirror is selected to verify the effectiveness of the proposed method, as shown in Fig.4. The distances from the centroid

of the diffractive film outer mirror O_{outer} and the inner circle mirror O_{inner} to the centroid of the diffractive film satellite O_{df} are set as 10 m and 5 m, respectively.
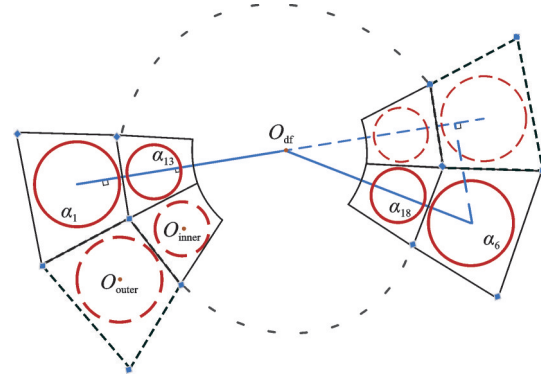

Fig.4   Diffractive film sub-mirror layout position

3.1   Performances of the proposed control method

The position of the imaging satellite is 100 meters in the direction of the film diffraction satellite vector. The orbit of the binary satellite is shown in Table 1.

Table 1   Detailed properties and characteristics of the binary satellite thin-film diffraction imaging system

Satellite	Semimajor axis a /m	Eccentricity e	Inclination i /(°)	RAAN $\varOmega$ /(°)	Argument of perigee ω /(°)	True anomaly f /(°)
Imaging satellite	6 878 000	0	45	0	0	30
Thin-film diffraction satellite	6 877 900	0	45	0	0	30

Four sub-mirrors are selected for numerical simulations, and their position parameters are shown in Table 2. The nominal inertia matrix of the

diffractive film sub-mirror α_i is

$$J_i =$$

$(10\,0.01\,0.01;\ 0.01\,11\,0.02;\ 0.01\,0.02\,10)\,\mathrm{kg \cdot m}^{2}$

The initial conditions of quaternion and angular velocity of each sub-mirror of the diffractive film satellite are: $Q_{bi}(0)=[\,1\quad 0\quad 0\quad 0\,]^{\mathrm{T}}$ and $\omega_{bi}(0)=0$ rad/s. The desired states of the tracking error quaternion and angular velocity are selected as $Q_{ei}=[\,1\quad 0\quad 0\quad 0\,]^{\mathrm{T}}$ and $\omega_{ei}(t)=0$ rad/s, respectively. In addition, the required maneuver angle is calculated by Eq.(4).

Table 2　Position parameters of the selected diffractive film sub-mirror α_i

Selected sub-mirrors	α_1	α_6	α_{13}	α_{18}
r_{mi}^{o}/m	$(10\quad 0\quad 0)$	$\left(-10\cos\dfrac{\pi}{6}\quad 10\sin\dfrac{\pi}{6}\quad 0\right)$	$(5\quad 0\quad 0)$	$\left(-5\cos\dfrac{\pi}{6}\quad 5\sin\dfrac{\pi}{6}\quad 0\right)$

The external disturbance of the diffractive film sub-mirror α_i is considered as

$$Td_i=([\,-0.01\quad -0.1\quad -0.01\,]^{\mathrm{T}}\cdot\sin(\omega_o t))\times 10^{-3}(\mathrm{N\cdot m})$$

where $\omega_o=\sqrt{\dfrac{\mu}{a^3}}$ is the average orbital angular velocity, a represents the semimajor axis and $\mu=398\,600.44$ km³/s² is the geocentric gravitational constant. The controller parameters are selected as follows.

$$j_i(0)=[\,10.4\quad 10.6\quad 10.5\quad 0.01\quad 0.01\quad 0.01\,]^{\mathrm{T}}(\mathrm{kg\cdot m^2})$$
$$Td_{Xi}(0)=0, K=\mathrm{diag}(0.15\quad 0.5\quad 0.15),$$
$$k=\mathrm{diag}(0.6\quad 0.5\quad 1.0),$$
$$\gamma=\mathrm{diag}(0.5\quad 0.05\quad 0.5\quad 0.01\quad 0.01\quad 0.01),$$
$$\tau=0.003, \varepsilon=0.3, \sigma=0.01$$

The control torque is limited to $[-0.2,0.2]\mathrm{N\cdot m}$.

The performances of the thin-film diffraction sub-array mirror controller are depicted in Figs.(5—10), respectively, where the numbers $i(i=1,6,13,18)$ are selected for presentation. As can be seen from Figs. 5 and 6, the diffractive film sub-mirror settles in approximately 200 s, and the tracking error quaternion and attitude angle approach the desired value in a well-behaved manner in a finite time. After 200 s, the upper bound of attitude angle error is $0.001°$ even though external disturbances induced by inertia uncertainties and variations affect the sub-mirror system. These two figures show that the controller can steer the diffractive film to the attitudes that point to desired imaging target and imaging satellite in a finite time.

Attitude angular velocity error and control torque of α_i are depicted in Figs.7 and 8, respectively. Fig.7 shows that the attitude angular velocity er-
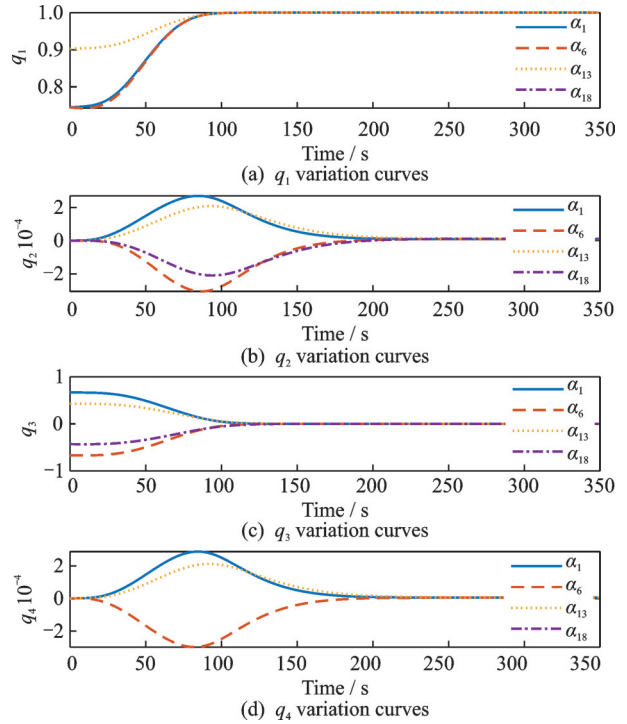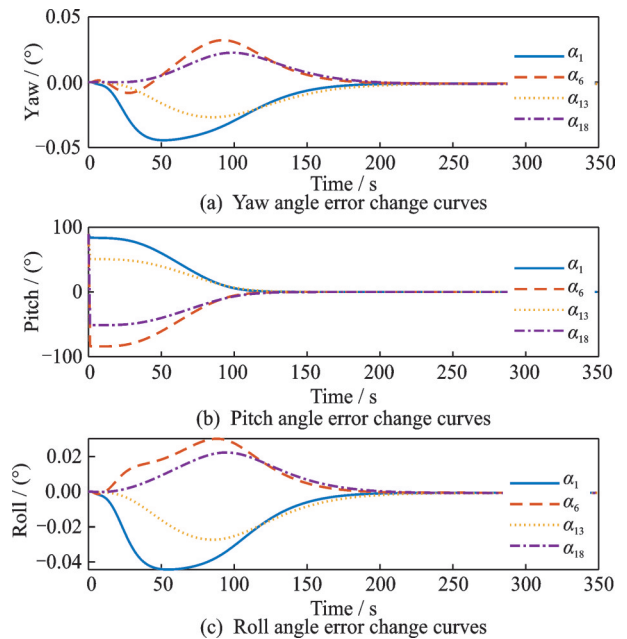

Fig.5　Error quaternion variation curve

Fig.6　Attitude angle error change curves

ror of α_i can reach the desired value in finite time. The chattering can be avoided effectively, as shown in Fig.8.
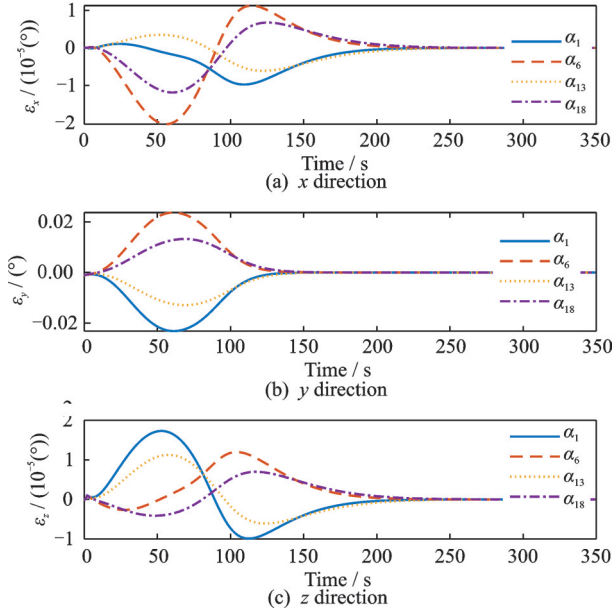

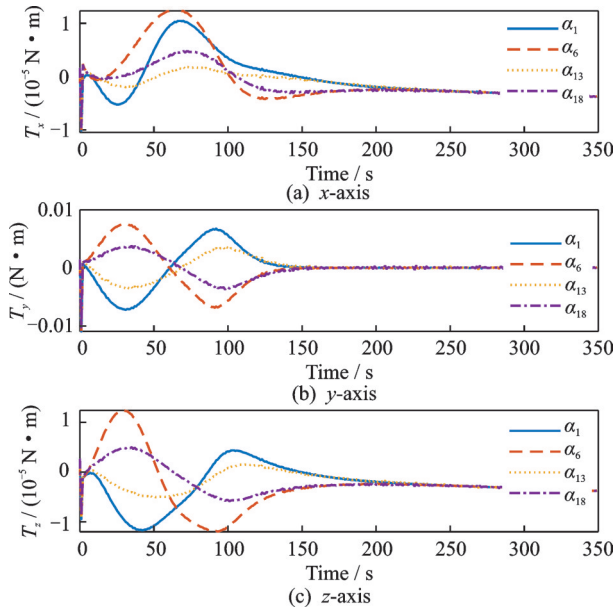Fig.7　Attitude angular velocity error change curves

Fig.8　Control torque curves

The nonlinear sliding mode adaptive controller of the diffractive film sub-mirror array can realize high-precision tracking and stable orientation of the posture of each sub-mirror.

Fig.9 shows the comparison of actual attitude angle of α_i and the desired attitude pointing angle, where α_i pitch$_b$ and α_i pitch$_t$ are actual and desired y-axis attitude angles of α_i, respectively.
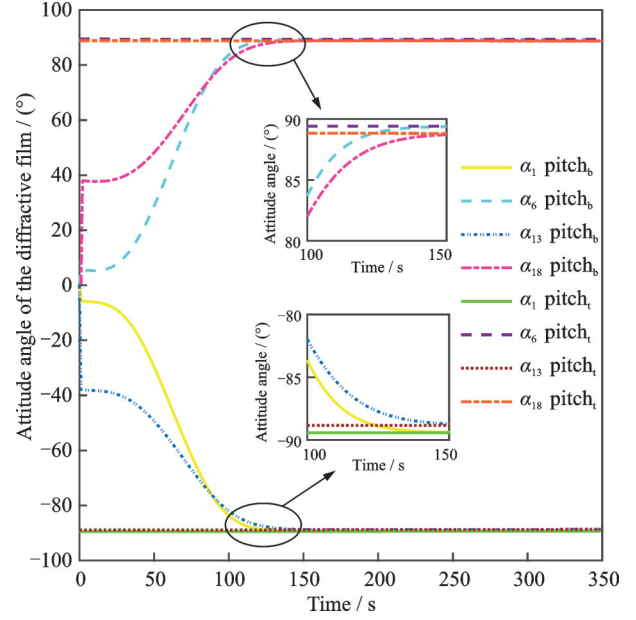

Fig.9　Comparison of actual and expected attitude angles of α_i

By comparison, it is more significant to show that within 150 s, the pitch angle converges to the desired tracking pointing angle.

Fig.10 shows that the adaptive estimated values of the disturbance torque converge into constant values over time. The uncertainty of the disturbance torque of each sub-mirror system is considered so that the control system can adapt to the parameters of satellite inertia and has strong robustness.
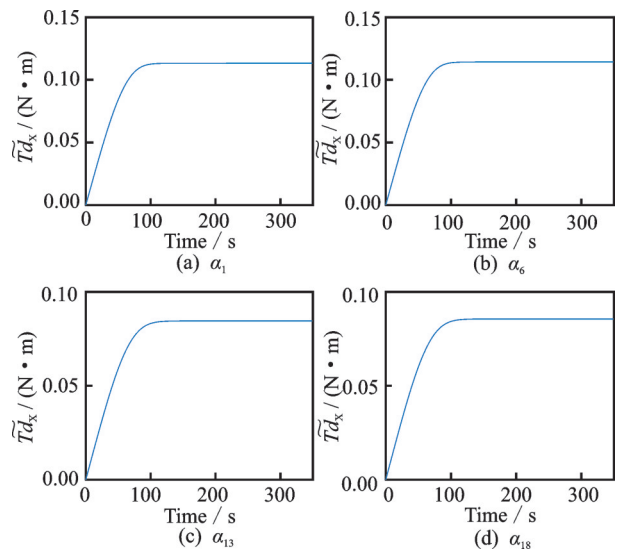

Fig.10　Disturbance torque estimates for α_i

3.2　Comparison with the PD control method

To show the performance advantages of the

controller proposed in a better comparison, a PD controller such as

$$T_i = -2\hat{K}_p \ln q_{ei} - \hat{K}_d \omega_{ei} - $$
$$f\Big(-(\omega_{ei} + C_i \omega_{ti})^\times J_i(\omega_{ei} + C_i \omega_{ti}) + $$
$$J_i(\omega_{ei}^\times C_i \omega_{ti} + C_i \dot{\omega}_{ti})\Big)$$

is introduced, where the parameters are chosen as $\hat{K}_p = 0.1$, $\hat{K}_d = 5$, and the control torque limit is $[-0.2, 0.2]$ N·m. One of the diffractive thin-film sub-mirrors, α_1, has been chosen as representative. For comparison, the simulation results for both controllers are shown in Fig.11. The subscript pb represents the PD controller, the subscript t the nonlinear sliding mode controller and the subscript b the expected value.

The diffraction film rotates around its pitch axis (Y-axis) to complete the orientation of the imaging satellite. Therefore, the pointing angle maximum steady-state error in the Y-axis and the 2-Norm of
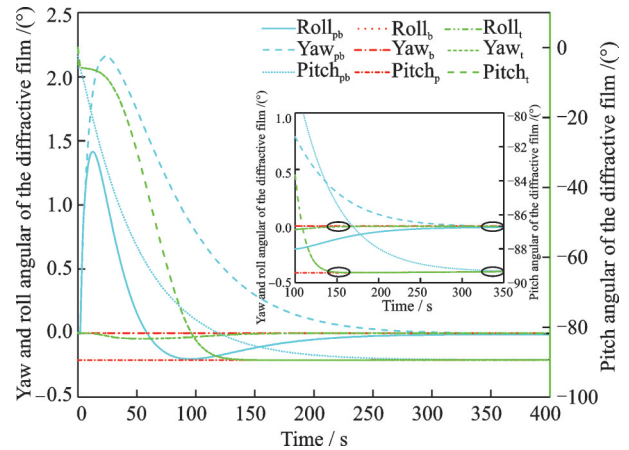

Fig.11   Controller performance comparison

the error in the three-axis attitude angle (RMS) of the diffracted film are taken as evaluation indicators.

The results are shown in Table 3. As can be seen from Table 3, the nonlinear sliding mode controller can achieve significant improvements in accuracy and convergence time compared to the PD controller.

Table 3   Performance comparison of two controllers

Controller	Convergence time /s	Pitch angular of the diffractive film maximum steady-state error /(°)	RMS
PD controller	350	0.04	0.05
Nonlinear sliding mode controller	150	0.01	0.01

It can be concluded from numerical results that the designed sliding mode controller with the continuous arctangent function can effectively suppress the chattering of the system and ensures the smooth convergence of the attitude angle. The control system can meet the accuracy requirements of the precise configuration for the heterogeneous binary satellite diffraction imaging system and has a fast response speed.

4   Conclusions

A nonlinear sliding mode adaptive controller is designed for the control problem of thin-film diffractive sub-mirrors with high-precision attitude tracking and pointing requirements in the binary satellite thin-film diffraction imaging system. In addition, the global stability of the controller is proved mathe-

matically. The designed controller can adapt to the parameters of satellite inertia and has strong robustness to disturbance torque. Finally, through numerical simulation and comparative verification, the following conclusions are drawn.

(1) The controller can meet the requirements of attitude control accuracy and stability in a heterogeneous binary satellite diffraction imaging system, which is posture tracking and orientation of imaging eyepieces by diffractive film sub-mirrors.

(2) The controller has strong robustness, which can adapt to the uncertainty of the rotational inertia and disturbance torque of each sub-mirror.

(3) The controller introduces a continuous arctangent function, which effectively eliminates the chattering of the system and further ensures the control accuracy of the pointing angle of the diffractive film sub-mirror.

References

[1] SUN X, WU X, CHEN W, et al. Dual quaternion based dynamics modeling for electromagnetic collocated satellites of diffraction imaging on geostationary orbit[J]. Acta Astronautica, 2019, 166: 52-58.

[2] PATERSON C, MUNRO I, DAINTY J C. A low cost adaptive optics system using a membrane mirror[J]. Optics Express, 2000, 6(9): 175-185.

[3] ENRIQUE J F, PABLO A. Membrane deformable mirror for adaptive optics: Performance limits in visual optics[J]. Optics Express, 2003, 11(9): 1056-1069.

[4] HYDE R A. Very large aperture diffractive telescopes[J]. Applied Optics, 1999, 38 (19): 4198-4212.

[5] DANIEL C, DAVID J. Technology for the next generation space telescope[C]//Proceedings of SPIE, [S.l.]: [s.n], 2000, 4013: 784-794.

[6] QU W, GU H, TAN Q. Design of refractive/diffractive hybrid optical elements for beam shaping with large diffraction pattern[J]. Chinese Optics Letters, 2016, 14(3): 64-67.

[7] TANDY W, ATCHESON P, DOMBER J, et al. MOIRE Gossamer space telescope—Structural challenges and solutions[C]//Proceedings of the 53rd AIAA/ASME/ASCE/AHS/ASC Structures, Structural Dynamics and Materials Conference 20th AIAA/ASME/AHS Adaptive Structures Conference 14th AIAA. [S.l.]: AIAA, 2012.

[8] SUN X, CHEN W, ZHOU B, et al. The isolation of co-located diffraction satellite for remote sensing after disaster[J]. Earthquake Engineering and Engineering Dynamics, 2019, 39(6): 18-26.

[9] LIU R, LIU M, SUN Z, et al. Impulse variance control for spacecraft autonomous rendezvous with an observer-based approach[J]. IMA Journal of Mathematical Control and Information, 2016, 35(1): 57-73.

[10] ZHAO J, WANG P, SUN Y, et al. Nonsingular fast terminal sliding mode control based on nonlinear disturbance observer for a quadrotor[J]. Transactions of Nanjing University of Aeronautics and Astronautics, 2022, 39(2): 219-230.

[11] LIU R, SUN Z, YE D. Adaptive sliding mode control for spacecraft autonomous rendezvous with elliptical orbits and thruster faults[J]. IEEE Access, 2017, 5: 24853-24862.

[12] WANG Y, JIANG C, CHEN H. Robust adaptive sliding mode control for nonlinear uncertain neutral delay system[J]. Transactions of Nanjing University of Aeronautics of Astronautics, 2005, 22(3): 259-263.

[13] CONG Binglong, CHEN Zhen, LIU Xiangdong. Adaptive sliding mode control for rigid spacecraft attitude tracking[J]. Acta Aeronautica et Astronautica Sinica, 2013, 34(3): 620-628. (in Chinese)

[14] SUN L, MA J. Robust adaptive attitude tracking control of spacecraft with constrained inputs[J]. Control and Decision, 2021, 36(9): 2297-2304.

[15] XU Guangde, YAN Xin, GOU Zhongqiu, et al. Research on attitude pointing tracking control for spacecraft based on relative orbit measurement[J]. Aerospace Control, 2017, 35(1): 54-59. (in Chinese)

[16] YIN Chunwu. Multi-loop attitude tracking control for capturing spacecraft[J]. Aerospace Control, 2018, 36(1): 8. (in Chinese)

[17] LI You, SHI Mengxin. Variable structure sliding mode control method for satellite attitude maneuver[J]. Journal of Xi'an Jiaotong University, 2022, 56(7): 56-66. (in Chinese)

[18] FENG Yushu, LIU Kun, FENG Jian. Finite time adaptive integral sliding mode control method for spacecraft attitude tracking[J]. Journal of University of Electronic Science and Technology of China, 2021, 50(4): 527-534. (in Chinese)

[19] WANG Z, LI Y. Rigid spacecraft robust adaptive attitude stabilization using state-dependent indirect Chebyshev pseudospectral method[J]. Acta Astronautica, 2020, 174: 94-102.

[20] SHAHNA M H, ABEDI M. Design of a finite time passivity based adaptive sliding mode control implementing on a spacecraft attitude dynamic simulator[J]. Control Engineering Practice, 2021, 114: 104866.

[21] WANG R, ZHANG Z, GUO L, et al. Effects of fabrication errors on diffraction efficiency for a diffractive membrane[J]. Chinese Optics Letters, 2016, 14(12): 120501.

[22] ZHANG J, LI M, YIN G, et al. Low-cost method of fabricating large-aperture, high efficiency, fresnel diffractive membrane optic using a modified moiré technique[J]. Chinese Optics Letters, 2016, 14(10): 10-14.

[23] ZHANG Renwei. Satellite orbit attitude dynamics and control[M]. Beijing: Beihang University Press, 1998. (in Chinese)

[24] LU K, XIA Y. Adaptive attitude tracking control for rigid spacecraft with finite-time convergence[J]. Automatica, 2013, 49(12): 3591-3599.

[25] ZHANG Zhiwen. Robust adaptive control of satellite attitude[D]. Harbin: Harbin Institute of Technology, 2009. (in Chinese)

［26］ ZOU A, KUMAR K D, HOU Z, et al. Finite-time attitude tracking control for spacecraft using terminal sliding mode and Chebyshev neural network[J]. IEEE Transactions on Systems, Man, and Cybernetics—Part B: Cybernetics, 2011, 41(4): 950-963.

［27］ DU H, LI S, QIAN C. Finite-time attitude tracking control of spacecraft with application to attitude synchronization[J]. IEEE Transactions on Automatic Control, 2011, 56(11): 2711-2717.

Authors   Ms. **MA Songjing** received her B.S. degree from Northeast Forestry University, Harbin, China, in 2020. She is now pursuing the M.S. degree in College of Aerospace and Civil Engineering, Harbin Engineering University. Her current research interests include integrated attitude and orbit, dual quaternion, adaptive sliding mode control, and adaptive robust control.

Dr. **SONG Xiangshuai** received his Ph.D. degree in dynamics and control from Dalian University of Technology, Dalian, China, in 2021. He is currently an assistant professor at College of Aerospace and Civil Engineering, Harbin Engineering University. His current research interests include shape and vibration control for smart antenna structures and satellite mission planning.

Author contributions   Ms. **MA Songjing** designed the study, complied the models, and wrote the manuscript. Dr. **SONG Xiangshuai** contributed to data analysis, result interpretation and manuscript revision. Mr. **LI Jun** contributed to the experiment analysis. Ms. **SUN Yuqi** contributed to the design and discussion of the study. Mr. **WANG Yuyao** contributed to the discussion and background of the study. All authors commented on the manuscript draft and approved the submission.

Competing interests   The authors declare no competing interests.

(Production Editor：WANG Jing)

基于非线性滑模的衍射薄膜自适应跟踪控制

马松靖[1]，宋祥帅[1]，李　军[2]，孙瑜奇[1]，王钰尧[1]

(1.哈尔滨工程大学航天与建筑工程学院,哈尔滨 150001,中国；2.中国船舶集团有限公司第七〇八研究所,上海 210110,中国)

摘要：设计了一种用于薄膜衍射成像系统的非线性滑模自适应控制器,以实现对大直径镜阵列中子阵列姿态的精确指向。通过推导基于误差四元数和角速度的运动学和动力学方程,设计衍射薄膜子镜阵列控制器进而实现精确指向。利用李雅普诺夫方法证明了控制器的全局稳定性。该控制器通过自适应地识别每个子镜系统的惯性矩阵,使其对有界扰动和惯性参数的变化具有鲁棒性。同时引入了连续反正切函数,有效防抖。仿真结果表明,在存在转动惯量矩阵不确定性和各种扰动的情况下,所设计的控制器能够保证各子镜中衍射膜的准确跟踪。

关键词：姿态跟踪;滑模控制;衍射成像;光学成像系统;李雅普诺夫函数